Hexadecadienyl Monolayers on Hydrogen-Terminated Si(111): Faster Monolayer Formation and Improved Surface Coverage Using the Enyne Moiety

7 AUTHORS, INCLUDING:

Sidharam Pujari
Wageningen University
29 PUBLICATIONS **309** CITATIONS

SEE PROFILE

Luc Scheres
Wageningen University
30 PUBLICATIONS **620** CITATIONS

SEE PROFILE

C.J.M. van Rijn
Wageningen University
108 PUBLICATIONS **1,844** CITATIONS

SEE PROFILE

Tobias Weidner
Max Planck Institute for Polymer Research
86 PUBLICATIONS **1,352** CITATIONS

SEE PROFILE

Hexadecadienyl Monolayers on Hydrogen-Terminated Si(111): Faster Monolayer Formation and Improved Surface Coverage Using the Enyne Moiety

Bart Rijksen,[†,⊥] Sidharam P. Pujari,[†,⊥] Luc Scheres,[†,‡] Cees J. M. van Rijn,[†] J. E. Baio,[§] Tobias Weidner,[§] and Han Zuilhof*[,†,‖]

[†]Laboratory of Organic Chemistry, Wageningen University, Dreijenplein 8, 6703 HB, Wageningen, The Netherlands
[‡]SurfiX B.V., Dreijenplein 8, 6703 HB, Wageningen, The Netherlands
[§]National ESCA and Surface Analysis Center for Biomedical Problems, University of Washington, Seattle, Washington 98195, United States
[‖]Department of Chemical and Materials Engineering, King Abdulaziz University, Jeddah, Saudi Arabia

Ⓢ Supporting Information

ABSTRACT: To further improve the coverage of organic monolayers on hydrogen-terminated silicon (H−Si) surfaces with respect to the hitherto best agents (1-alkynes), it was hypothesized that enynes (H−C≡C−HC=CH−R) would be even better reagents for dense monolayer formation. To investigate whether the increased delocalization of β-carbon radicals by the enyne functionality indeed lowers the activation barrier, the kinetics of monolayer formation by hexadec-3-en-1-yne and 1-hexadecyne on H−Si(111) were followed by studying partially incomplete monolayers. Ellipsometry and static contact angle measurements indeed showed a faster increase of layer thickness and hydrophobicity for the hexadec-3-en-1-yne-derived monolayers. This more rapid monolayer formation was supported by IRRAS and XPS measurements that for the enyne show a faster increase of the CH_2 stretching bands and the amount of carbon at the surface (C/Si ratio), respectively. Monolayer formation at room temperature yielded plateau values for hexadec-3-en-1-yne and 1-hexadecyne after 8 and 16 h, respectively. Additional experiments were performed for 16 h at 80° to ensure full completion of the layers, which allows comparison of the quality of both layers. Ellipsometry thicknesses (2.0 nm) and contact angles (111−112°) indicated a high quality of both layers. XPS, in combination with DFT calculations, revealed terminal attachment of hexadec-3-en-1-yne to the H−Si surface, leading to dienyl monolayers. Moreover, analysis of the Si_{2p} region showed no surface oxidation. Quantitative XPS measurements, obtained via rotating Si samples, showed a higher surface coverage for C_{16} dienyl layers than for C_{16} alkenyl layers (63% vs 59%). The dense packing of the layers was confirmed by IRRAS and NEXAFS results. Molecular mechanics simulations were undertaken to understand the differences in reactivity and surface coverage. Alkenyl layers show more favorable packing energies for surface coverages up to 50−55%. At higher coverages, this packing energy rises quickly, and there the dienyl packing becomes more favorable. When the binding energies are included the difference becomes more pronounced, and dense packing of dienyl layers becomes more favorable by 2−3 kcal/mol. These combined data show that enynes provide the highest-quality organic monolayers reported on H−Si up to now.
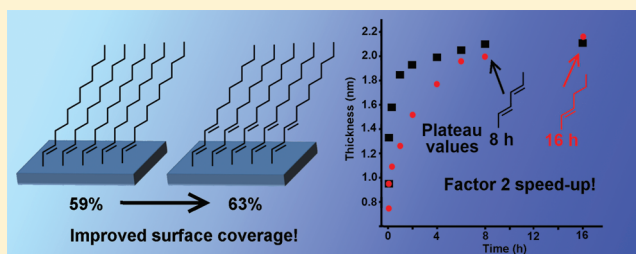
■ INTRODUCTION

Long-term passivation of oxide-free silicon surfaces can be achieved by the covalent attachment of self-assembled monolayers onto hydrogen-terminated silicon surfaces (H−Si). Not only can these thin organic layers protect the surface from oxidation, they also form a versatile scaffold for (bio)functionalization.[1−6] Many methods and procedures to produce these layers have been described in the literature, including thermal[7,8] and UV[9−12] methods, electrochemistry,[13,14] and chemomechanical scribing.[15,16] However, under those reaction conditions, side reactions might occur, thereby reducing the quality of the produced layers.[17,18] Milder

methods, which invoke a substantially lower energy input, have been shown to overcome these issues, although at cost of longer reaction times.[19,20] Hence, a reduction of the reaction time under these mild reaction conditions, while maintaining the oxide-free nature of the organic monolayer−silicon interface, might bring application of these layers in (bio)-electronic devices within reach.[21−25]

Scheme 1. Mechanistic Hypothesis That Initiated Study of Enynes for Monolayers on H−Si(111)[a]
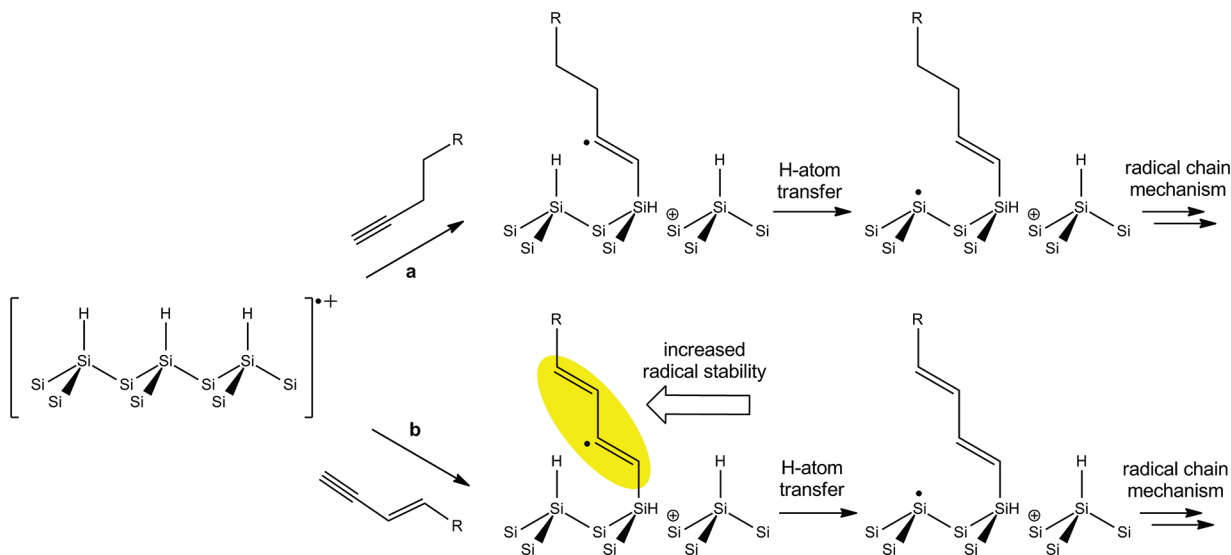
[a]Nucleophilic attack of (a) 1-alkynes and (b) 3-en-1-ynes to delocalized radical cations at the silicon surface result in the formation of β-carbon radicals. Subsequent transfer of a hydrogen atom from a neighboring Si−H site then results in the formation of a surface-centered radical.

For these potential applications, the stability of the oxide-free monolayer−silicon interface is one of the most important properties, for which oxidation is a hampering factor both during and after the modification process.[26,27] During the formation of the, not yet complete, monolayer, oxidation by traces of oxygen present in the precursor or reaction flask might be relatively fast and competes with the precursors for reactive surface sites. After completion of the monolayer, the oxidation rate is relatively slow due to the limited diffusion of oxygen through the monolayer,[28] but even there, only a small fraction of defects in the monolayer is already sufficient to cause detectable amounts of oxide after prolonged storage in ambient conditions.[29] To further improve the stability of the oxide-free monolayer−silicon interfaces, both oxidation routes need to be suppressed via a combination of faster attachment and a higher packing density.

One of the current theories that explains mild attachment involves initiation by nucleophilic attack of the precursors to delocalized silyl radical cations at the H−Si surface (see Scheme 1).[5,6,30] Hence, better nucleophiles will improve the initial attack on the delocalized radical cations and therefore facilitate C−Si bond formation. In addition, recent studies have shown that stabilizing the β-carbon radical intermediate by a neighboring π-system speeds up the propagation of the radical chain mechanism and thereby monolayer formation.[31−33] In accordance with the above, a significant higher reactivity of ω-alkynes as compared to ω-alkenes has been demonstrated on H−Si(100) and H−Si(111) surfaces.[34,35]

Besides the reactivity, also the shape and footprint of the precursor are important parameters, as both can have a tremendous influence on the packing, and thus on the stability of the layer.[36] Limited by steric constraints and unfavorable conformations of the carbon chains near the surface, numerous studies have reported a maximum surface coverage of 50−55% for alkyl monolayers on Si(111).[7,9,35,37−42] However, by introducing moieties with a smaller van der Waals radius than a regular CH$_2$-group, that is, a smaller footprint, packing densities as high as ~67% have been obtained for long alkoxyl (Si−O−C) monolayers[40,43,44] and for C$_{18}$ alkenyl (Si−C=C)

monolayers on H−Si(111).[19,35,36] Obviously, this is a clear indication that even minor structural differences in the linkage can have a major effect on the overall monolayer structure. In addition, regarding the long-term stability of the oxide-free interface, we note that a higher surface coverage will not only slow diffusion of water and oxygen through the monolayer, but will also result in slightly reduced numbers of unreacted H−Si sites at the interface.

All of these findings encouraged us to design two new precursors with a further increased reactivity and the proper geometrical requirements. As can been seen in Scheme 1, both candidate structures (hexadec-3-en-1-yne and 1,3-hexadeca-diyne) possess a conjugated reactive terminal functionality, which is expected to enhance the nucleophilic attack at the silicon surface and might improve subsequent stabilization of the β-carbon radical intermediate by the neighboring π-system. Furthermore, because CH=CH moieties have a significantly smaller footprint than CH$_2$−CH$_2$ moieties, the smaller van der Waals radius of both linkages to the silicon surface (Si−HC=CH−HC=CH− and Si−HC=CH−C≡C−, respectively) meets the requirements to obtain high surface coverage organic monolayers.

In a recent photospectroscopic study, the reactivity of these two candidate structures toward silyl radicals has been investigated.[31] It was shown that hexadec-3-en-1-yne and 1,3-hexadecadiyne are both at least 30 times more reactive than 1-alkynes. However, preliminary results of monolayer-forming experiments showed that diynes polymerize under monolayer-forming conditions, which precludes their use in this.

The above ideas and results stimulated us to investigate the kinetics of monolayer formation with hexadec-3-ene-1-yne on hydrogen-terminated Si(111) in detail. To visualize a possible enhanced reactivity of the 3-ene-1-yne functionality as compared to 1-alkynes, 1-hexadecyne-derived monolayers were used as a reference. The kinetics of the surface attachment reactions were followed by studying partially complete monolayers obtained after fixed times by static contact angle measurements, ellipsometry, infrared reflective absorption spectroscopy (IRRAS), and X-ray photoelectron spectroscopy

(XPS). Next, to reveal the influence of the structurally different linkage to the H–Si(111) substrate (Si–C≡C–C≡C versus Si–C≡C) on the quality and structure of the final monolayers, fully completed hexadecadienyl and hexadecenyl monolayers were thoroughly studied by additional quantitative XPS measurements involving rotating Si samples to exclude crystal reflection effects,[35,39] DFT calculations, attenuated total reflection (ATR), and near-edge X-ray absorption fine structure (NEXAFS) measurements. Finally, a combined ab initio and molecular mechanics molecular modeling study was undertaken to provide insight into the subtle chemical and structural differences responsible for the observed reactivity and quality difference between alk-3-ene-1-yne and in 1-alkyne-derived monolayers. The resulting picture clarifies the potential of novel, high-reactivity moieties for the attachment of organic monolayers onto H–Si surfaces.

■ MATERIALS AND METHODS

Materials. Bis(trimethylsilyl)-1,3-butadiyne (96%), 1-bromododecane (99%), potassium fluoride dihydrate, dimethylformamide (DMF), hexamethylphosphoramide (HMPA), methyllithium/LiBr in diethylether (1.6 M), di-isobutylaluminumhydride in pentane (1.6 M), dimethoxyethane (DME) (anhydrous), n-butyllithium in pentane (1.6 M), acetone (semiconductor grade VLSI PURANAL Honeywell 17617), and sulfuric acid (95–97%) were obtained from Sigma-Aldrich. From other sources we purchased hydrogen peroxide (Acros Organics, 35%), ammonium fluoride (Riedel-de Haën, 40%, semiconductor grade VLSI PURANAL Honeywell 17600), deionized water (resistivity 18.3 MΩ cm), and pentane (VWR, 95%). 1-Hexadecyne (90%, ABCR, Germany) was purified by column chromatography (hexane) to remove trace amounts of 1-bromoalkane, and subsequently distilled twice under reduced pressure before use. Silicon wafers were (111)-oriented, single-side or doubly polished (500–550 μm thick, n-type doping by phosphorus), and have a resistivity of 2.0–8.0 Ω cm (Siltronix, France).

Equipment. NMR spectra were recorded on a Bruker Avance III with an inverse broadband probe running at 400 MHz, with C_6D_6 as solvent. Hexadeca-3-ene-1-yne was purified by HPLC (Shimadzu, ALLTIMA C18 5U column, MeOH, 15 mL/min, UV detection at 215 nm).

Synthesis of Hexadeca-3-ene-1-yne. This compound was synthesized according to a literature procedure,[45] using 1-tris-(trimethyl)silyl-1,3-hexadeca-diyne[46,47] as precursor, and purified by prep-HPLC (C_{18} reversed phase/MeOH) to achieve 99.9% purity as determined with GC–MS. Yield: 90%. ^{1}H NMR (400 MHz, C_6D_6): δ 0.91 (t, J = 6.8 Hz, 3H), 1.13–1.29 (m, 20H), 1.82 (m, 2H), 3.01 (s, 1H), 5.52 (d, J = 15.6 Hz, 1H), 6.18 (m, 1H). ^{13}C NMR (100 MHz, C_6D_6): δ 14.39 (CH$_3$), 23.15, 29.00, 29.14, 29.42, 29.59, 29.85, 30.01, 30.13, 30.16, 30.74, 33.31, 92.79 (HC≡$\underline{C}$–), 105.08 (H$\underline{C}$≡C–), 110.58 (≡C–$\underline{C}$H=), 146.12 (C=$\underline{C}$H–CH$_2$). MS (EI): m/z (%) 220 (1) [M$^+$], 135 (23), 121 (37), 107 (38), 93 (74), 79 (100), 67 (54), 55 (54).

Hydrogen-Terminated Si(111) Surfaces (H–Si(111)). H–Si(111) was prepared by chemical etching as previously reported.[48,49] All liquid reagents were continuously purged with an argon flow. An n-type Si (111) wafer with a 0.2° miscut angle along ⟨112⟩ was first cut (10 × 10 mm^2) and subsequently cleaned in a sonication bath with acetone and then with Milli-Q water (resistivity >18 MΩ cm). The Si wafer was oxidized in freshly prepared piranha solution (H$_2$SO$_4$/H$_2$O$_2$ 3:1) for at least 20 min. After piranha treatment, the substrates were immersed immediately in water and rinsed thoroughly, followed by drying with a stream of argon. Subsequently, the substrates were etched in an argon-saturated 40% aqueous NH$_4$F solution for 15 min, rinsed by Milli-Q water, and finally dried with a stream of argon. The H–Si surfaces were studied by X-ray photoelectron spectroscopy (XPS) and atomic force microscopy.

Preparation of Hexadec-3-ene-1-yne- and 1-Hexadecyne-Derived Monolayers on H–Si(111). *Kinetic Studies.* After being

etched, the samples were rinsed with argon-saturated water, and finally blown dry with a stream of argon. These samples were then immediately transferred to the inert atmosphere glovebox. Next, the surface was covered with a few drops of neat 1-hexadecyne or hexadeca-3-ene-1-yne. The reactions were performed at room temperature under ambient light (i.e., standard fluorescent lamps in the fume hood were on). To stop the reaction, the sample was removed from the glovebox and immediately extensively rinsed with pentane and CH$_2$Cl$_2$. The sample was then sonicated for 5 min in CH$_2$Cl$_2$ to remove physisorbed molecules, after which the samples were blown dry with a stream of dry argon.

Quality Studies. High-quality monolayers were produced in a fume hood setup described in literature.[35,48] A three-necked flask was charged with 2 mL of 1-hexadecyne or hexadeca-3-ene-1-yne and was purged with argon under reduced pressure for 30 min, while being heated up to 80 °C. The freshly etched and dried surface was then quickly transferred into the flask, which was immediately depressurized again. The reaction mixture was kept at 80 °C overnight. The sample was then removed from the flask and immediately extensively rinsed with pentane and CH$_2$Cl$_2$, sonicated for 5 min in CH$_2$Cl$_2$ to remove physisorbed molecules, and blown dry with a stream of dry argon.

Monolayer Characterization. *Contact Angle Measurements.* Contact angle measurements were performed on a Krüss DSA 100 contact angle goniometer with an automated drop dispenser and image video capture system. The static contact angles of six small droplets (3.0 μL volume of deionized water), dispensed on modified silicon surfaces, were determined using the implemented Tangent 2 fitting model. The digital drop images were processed by the image analysis system, which calculated both the left and the right contact angles from the drop shape with an accuracy of ±1.0°.

Ellipsometry. The thickness of the modified silicon surfaces (in the dry state) was measured using a rotating analyzer ellipsometer of Sentech Instruments (Type SE-400), operating at 632.8 nm (He–Ne laser), and an angle of incidence of 70°. The optical constants of the substrate were determined with a piece of freshly etched H–Si(111) (n = 3.819 and k = 0.057). The thicknesses of the monolayers were determined with a planar three-layer (ambient, monolayer, substrate) isotropic model with a refractive index for the organic monolayers of 1.46. The reported values for the layer thickness are the average of eight measurements taken at different locations on the substrate with an error <1 Å.

X-ray Photoelectron Spectroscopy (XPS). XPS measurements were performed using a JPS-9200 photoelectron spectrometer (JEOL, Japan). A monochromatic Al Kα X-ray source (h_ν = 1486.7 eV) 12 kV and 20 mA using an analyzer pass energy of 10 eV was used. The base pressure in the chamber during measurements was 3×10^{-7} Torr, and spectra were collected at room temperature. The intensity of XPS core level electron was measured as the peak area after standard background subtraction according to the linear procedure. The takeoff angle φ (angle between sample and detector) of 80° is defined with a precision 1°. The typical sample size was 1 × 1 cm^2. For a precise determination of the atomic C/Si ratio of organic monolayers on Si(111), the influence of X-ray photo diffraction (XPD) on the XPS signal had to be accounted for.[35,39] Therefore, the samples were rotated 360° around the surface normal, yielding rotationally averaged C$_{1s}$ and Si$_{2p}$ emissions to obtain a truly quantitative C/Si ratio, which is now independent of the orientation of the sample. As our sample holder only allows rotation of the samples at a takeoff angle of 90°, we used nonmonochromatic Al Kα X-ray radiation (twin source) at 10 kV and 15 mA with an analyzer pass energy of 50 eV and a takeoff angle of 90° for these measurements. All spectra were corrected with a slight linear background before fitting. All XPS spectra were evaluated using the Casa XPS software (version 2.3.15). All binding energies are referenced relative to the main hydrocarbon (CH$_2$) peak with a binding energy of 285.0 eV.

Near-Edge X-ray Absorption Fine Structure (NEXAFS). NEXAFS spectra were collected at the National Synchrotron Light Source (NSLS) U7A beamline at Brookhaven National Laboratory, using an
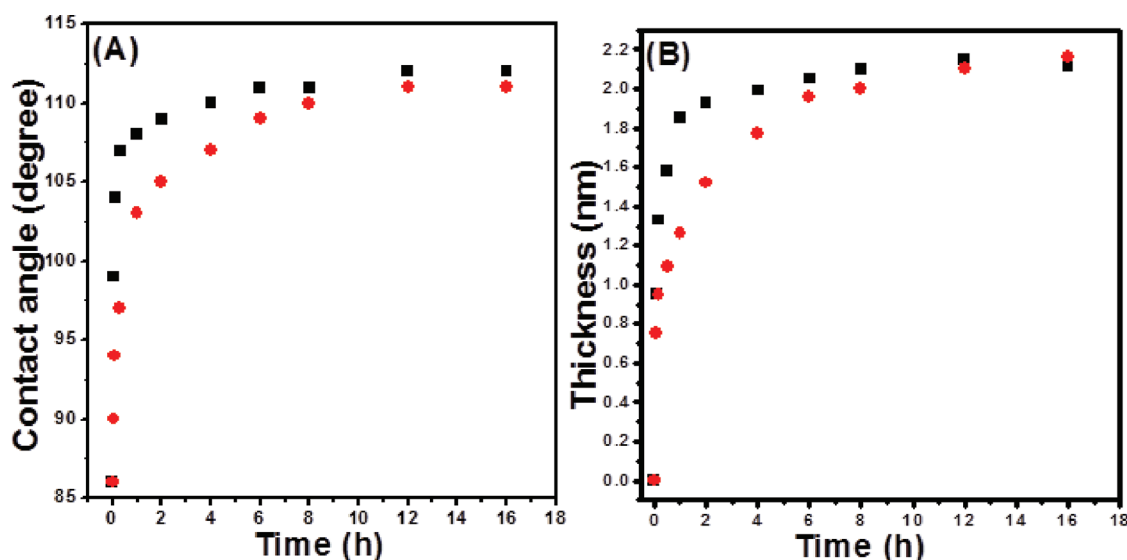
Figure 1. (A) Static water contact angles (±1°) and (B) layer ellipsometric thicknesses (±0.1 nm) of hexadec-3-en-1-yne (■) and 1-hexadecyne (●) layers versus the reaction times at room temperature. Each data point represents the average value of two separately prepared monolayers (see the Supporting Information).

elliptically polarized beam with ~85% p-polarization. This beamline utilizes a monochromator and 600 L/mm grating providing a full-width at half-maximum (fwhm) resolution of ~0.15 eV at the carbon K-edge. The monochromator energy scale was calibrated using the intense C 1s−π* transition at 285.35 eV of a graphite transmission grid placed in the path of the X-rays. Partial electron yield was monitored by a detector with the bias voltage maintained at −150 V. Samples were mounted to allow rotation and allow changing the angle between the sample surface and the synchrotron X-rays. The NEXAFS angle is defined as the angle between the incident light and the sample surface. The spectra were brought to the standard form by linear pre-edge background subtraction and normalizing to the unity edge jump defined by a horizontal plateau 40−50 eV above the absorption edge.

Fourier Transform Infrared Reflection Absorption Spectroscopy (FT-IRRAS). IRRAS spectra were recorded on a Bruker Tensor 27 FT-IR spectrometer using a variable-angle reflection unit (Auto Seagull, Harrick Scientific). A Harrick grid polarizer was installed in front of the detector and was used to record spectra with p-polarized (parallel) radiation with respect to the plane of incidence at the sample surface. All spectra were obtained at an incident angle of 68° (2048 scans). The resolution was set at 1 cm^{-1} per modulation center. The final spectra were obtained using a piranha-oxidized reference surface as background. Data were collected as differential reflectance versus wavenumber. All spectra were recorded at room temperature in dry atmosphere. A linear baseline correction was applied.

Attenuated total reflection (ATR). Infrared spectra were acquired using a Bruker spectrometer (model Tensor 27) equipped with a Harrick ATR accessory (Harrick Scientific Co.) and an FTIR spectrometer equipped with liquid nitrogen cooled mercury cadmium telluride (MCT) detectors. A wire-grid Harrick polariser was placed in front of the sample to measure p- (parallel) or s- (perpendicular) polarization with respect to the light incidence plane. The spectrometer was purged with dry nitrogen to minimize the contribution of moisture and CO_2 to the recorded spectra. Double side polished single crystal n-Si(111) wafers were cut into pieces of 5 × 1 cm^2 and polished to obtain ATR crystals with 45° angles with respect to the large parallel bevel faces, producing approximately 100 internal optical reflections of the incident beam. The reflection spectra of the samples were in the wavenumber range 4000 to 560 cm^{-1} and resolution of 1 cm^{-1} spectra where the average of 10000 scans. The unit of absorbance intensity was defined as −log(R/Ro), where R and Ro are the reflectivity of the substrate with and without the monolayer, respectively.

Computational Procedures. *XPS Binding Energies.* XPS binding energies were estimated by calculating the orbital energies of molecular analogues of C_{16} chains attached to a silicon surface. A $Si(SiH_3)_3$ group was attached to specifically mimic the Si−C bond.[50] The geometries were optimized with B3LYP/6-311G(d,p), using the Gaussian 09 package.[34] The carbon binding energies were then estimated by calculating the 1s core energy versus the average of the 2p valence orbital energies (mimicking the Fermi level).

Monolayer Simulations. Unit cells were constructed and expanded to supercells of 12 × 12 units (33%, 50%, 67%, and 75% surface coverage) and 10 × 15 units (60% surface coverage), following literature procedures.[35] The geometries were optimized using the polymer consistent force field (PCFF) (bottom two rows of Si atoms were constrained) as implemented in the Discover package in Materials Studio, using the ultrafine settings of the smart minimizer routine (line width 0.01 and convergence 10^{-5}, VdW and coulomb, atom centered and long-range correction switched off).[35] All G3 calculations of the binding energies of the chains to the surface were performed using the Gaussian 09 package.

■ RESULTS AND DISCUSSION

1. Reactivity Difference of 3-En-1-ynes and 1-Alkynes onto H−Si(111). To study the reactivity difference of alkynes and alk-3-en-1-ynes toward oxide-free hydrogen-terminated Si(111) (H−Si(111)) surfaces, the kinetics of monolayer formation under ambient conditions were explored by analyzing the resulting (partial) monolayers after different reaction times. To minimize the effect of competing oxidation reactions induced by water and oxygen, the experiments were performed in a glovebox under argon atmosphere. Precursors and freshly etched H−Si(111) were deoxygenized by three or more freeze−pump−thaw cycles before transferring them into the glovebox. The reaction was started by covering the freshly etched surfaces with 1 or 2 drops of precursor. The surfaces were then allowed to react for the appropriate time at a constant temperature of 20 °C. Subsequently, the resulting (partial) monolayers were analyzed by static water contact angle measurements, ellipsometry and X-ray photoelectron spectroscopy (XPS), and infrared reflection−absorption spectroscopy (IRRAS). As shown in Figure 1A, for both precursors,
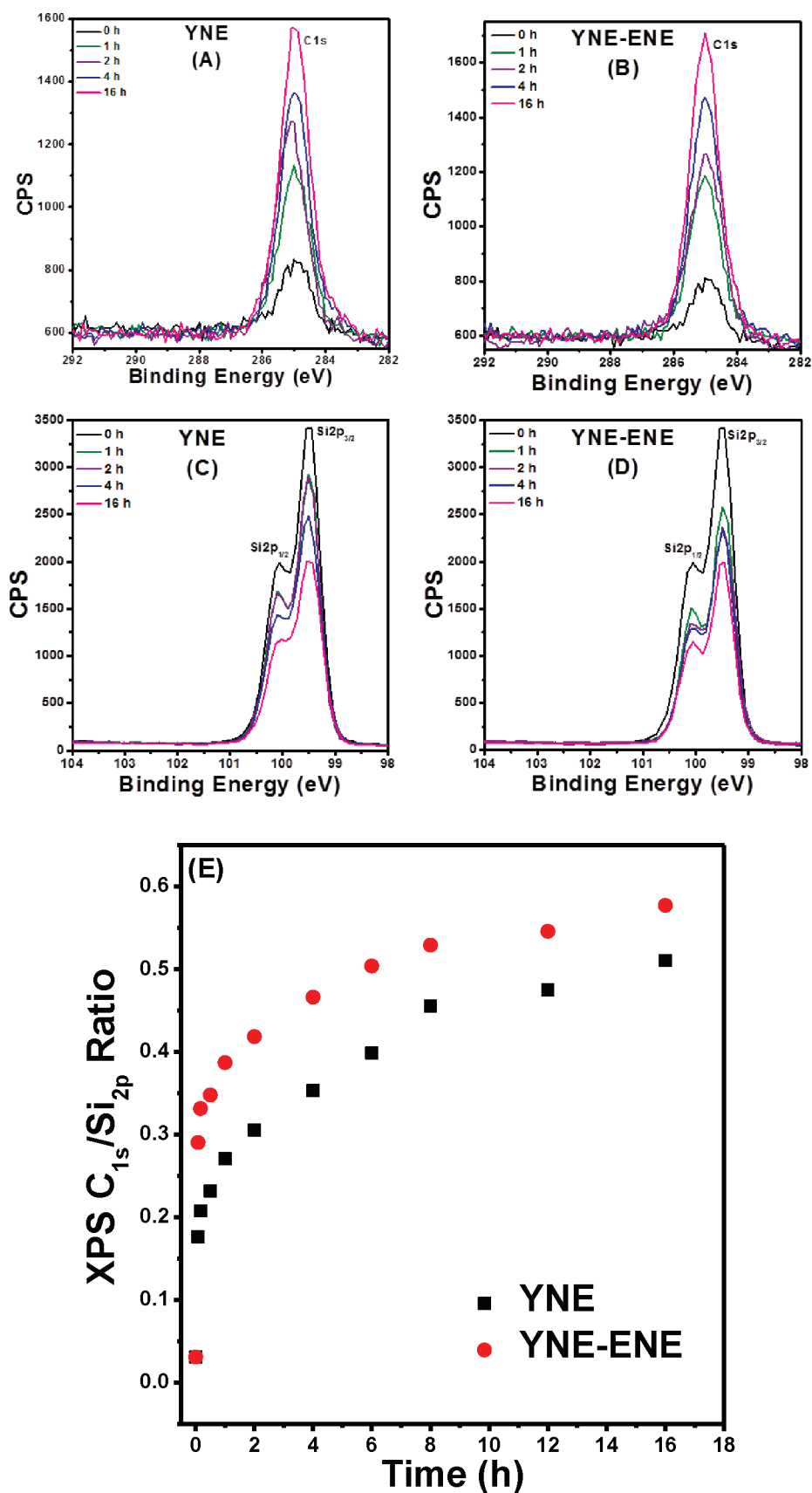
Figure 2. XPS spectra of the C_{1s} (A and B) and Si_{2p} region (C and D) of monolayers on H−Si(111) derived from 1-hexadecyne and hexadec-3-en-1-yne, respectively; and C_{1s}/Si_{2p} ratios in time (E).
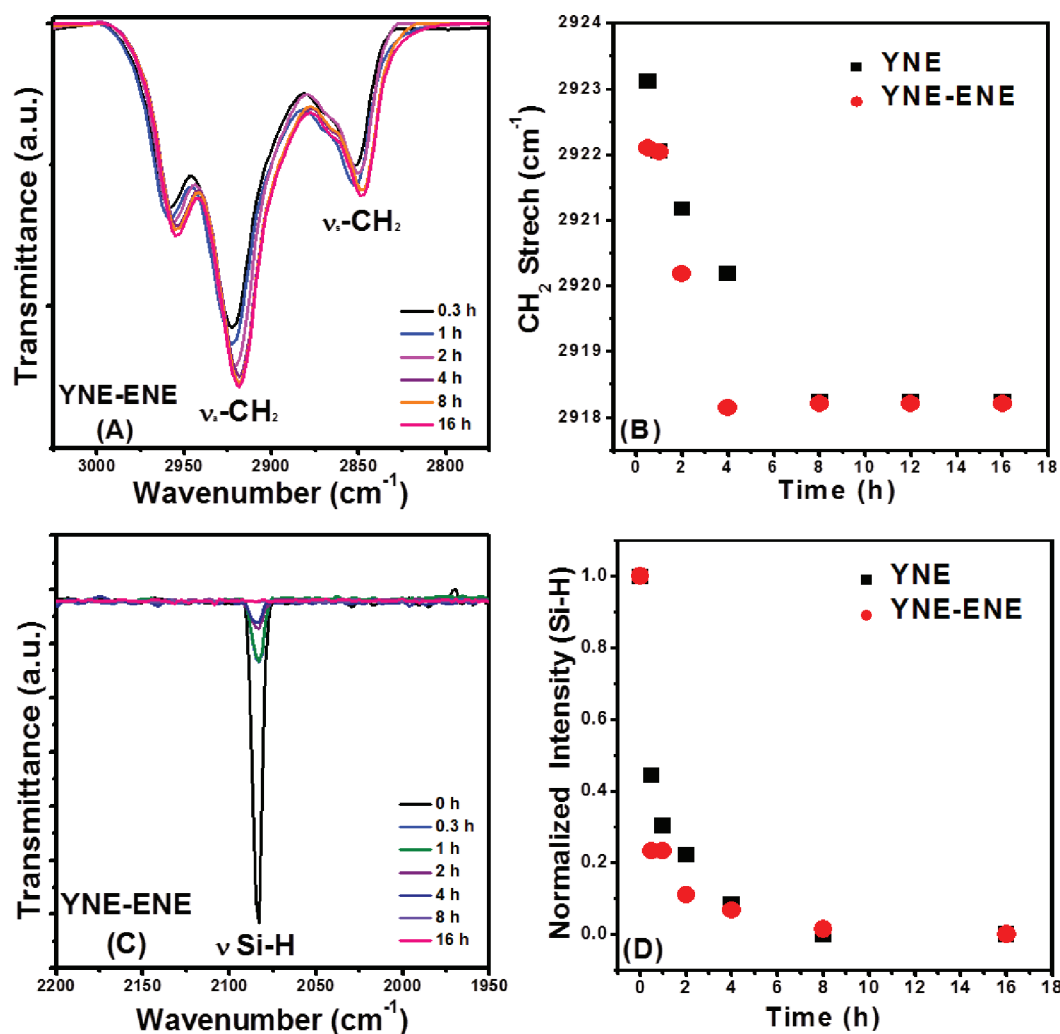
Figure 3. IRRAS data of 1-alkyne-derived and 3-en-1-yne-derived monolayers on H−Si(111) at ambient condition as a function of reaction time: (A) CH$_2$ stretch region of 3-en-1-yne in time, (B) CH$_2$ stretch frequencies of 3-en-1-yne and 1-yne monolayers in time, (C) Si−H stretch region of 3-en-1-yne in time, and (D) Si−H stretch normalized peak areas in time.

the static contact angles gradually increase in time, while monolayer formation proceeds faster with hexadec-3-en-1-yne than with 1-hexadecyne. With hexadec-3-en-1-yne, the plateau value of 111−112°, indicative of hydrophobic and densely packed organic monolayers,[7,19,35,48,51] was already reached after 8 h, while for 1-hexadecyne these values were only obtained after increasing the reaction time to 16 h. This demonstrates a considerable reactivity difference between both precursors. As expected, this difference in reactivity was also displayed by the ellipsometry measurements (see Figure 1B), which show significant differences in the growth of the layer thickness over time. The hexadecadienyl monolayers reached a thickness of 1.9 nm after 2 h, while hexadecenyl monolayers were then only 1.5 nm thick. The plateau value of 2.1 (±0.1 nm) nm for hexadec-3-en-1-yne was reached after 8 h, whereas it took the 1-hexadecyne at least 16 h.

To monitor the actual formation of the organic monolayer, the contributions of the Si$_{2p}$ and C$_{1s}$ core levels were studied in time by XPS narrow scans. For both precursors, the Si$_{2p}$ signal rapidly decreases in time, which coincides with an increase of the carbon signal at 285 eV (Figure 2A and B). This is a clear indication of the formation of an organic monolayer. Furthermore, the Si$_{2p}$ narrow scans of both partial and complete organic monolayers show no visible traces of oxygen at the silicon surface, demonstrating the success of the stringent oxygen-excluding conditions required to study the kinetics of monolayer formation in detail, and to obtain high-quality organic monolayers on oxide-free H−Si (see Figure 2C and D).[20,35] Finally, from Figure 2E (which shows the C$_{1s}$/Si$_{2p}$ ratios in time), it becomes clear that the carbon buildup of the 3-en-1-yne layers is faster than of the 1-yne counterpart. In fact, the amount of carbon after 16 h of reaction of 1-yne is in the case of the 3-en-1-yne already achieved after 6−8 h of reaction. This indicates a speed-up of a factor of ∼2, which is in agreement with the contact angles and the ellipsometric thicknesses discussed earlier.

To obtain detailed information about the molecular order of the (partial) monolayers in time, IRRAS measurements were carried out. As can be seen in Figure 3A and B, the intensities of the antisymmetric (ν_a) and symmetric (ν_s) methylene stretching vibrations grow gradually in time for both precursors, clearly displaying the increasing amount of carbon chains at the surface. Furthermore, upon completion of the monolayers, for both types of monolayer, the antisymmetric and symmetric CH$_2$ stretching frequencies shift from 2923 to 2918 cm^{-1} and from 2853 to 2848 cm^{-1}, respectively. These optimal
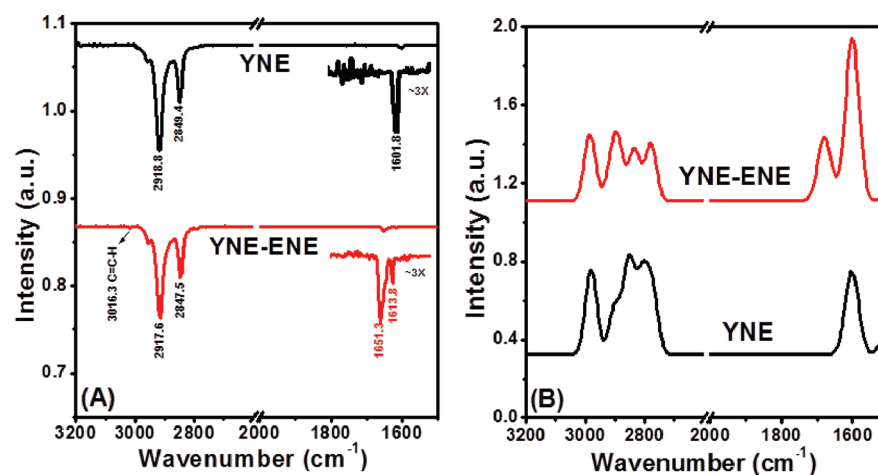
Figure 4. (A) ATR of hexadec-3-en-1-yne (red)- and 1-hexadecyne (black)-derived monolayers on H−Si(111) at 80 °C; and (B) frequencies from G3 calculations of carbon chains attached to silicon clusters.
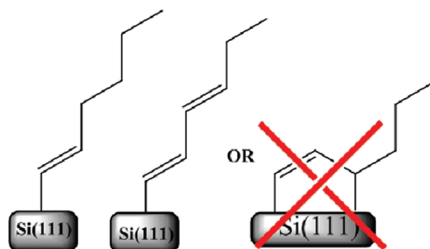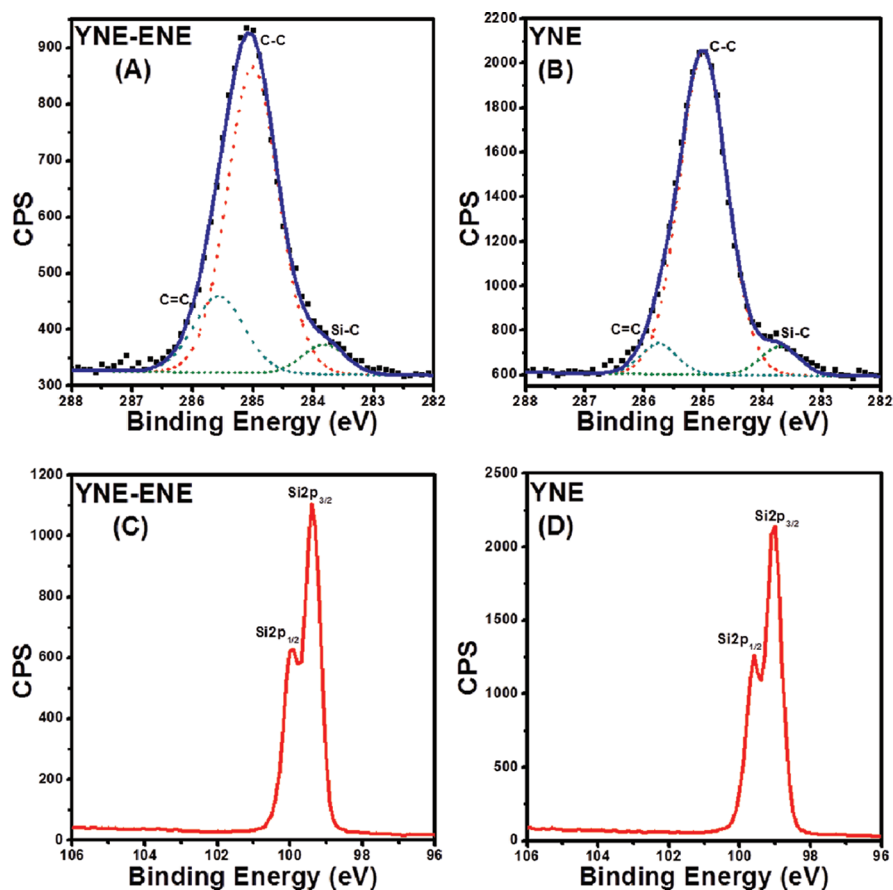
Figure 5. C$_{1s}$ (A,B) and Si$_{2p}$ (C,D) XPS narrow scan spectra of the H−Si(111) surface after modification (80 °C, 16 h) with hexadec-3-en-1-yne and 1-hexadecyne, respectively.

frequencies were obtained after 4 h for the hexadec-3-en-1-yne and after 8 h for the 1-hexadecyne. This difference of speed (~factor 2) is in line with the contact angle and ellipsometry data in Figure 1. We note that these frequencies correspond to highly ordered organic monolayers and are for 1-hexadecyne in good agreement with literature.[51−53] Moreover, the gradual disappearance of a detectable Si−H stretching vibration at 2083 cm⁻¹ (Figure 3C and D) confirms the formation of a monolayer by adsorption of the precursors onto H−Si(111).[19,35] The initial rate difference is in line with the speed-up demonstrated earlier. However, loss of a detectable Si−H stretching vibration prevents accurate comparison of the speeds at longer reaction times.

2. High-Quality Hexadecedienyl and Hexadecenyl Monolayers on H−Si(111).

After we confirmed the considerably higher reactivity of the 3-en-1-yne moiety toward H−Si(111) as compared to the 1-yne moiety, the quality of the both final monolayers was studied in more detail. To ensure completion of the monolayer formation, that is, to minimize the number of defects, more stringent reaction conditions (16 h at 80 °C) were chosen. Static water contact angles of 111−112°, advancing contact angles of 116−117°, receding contact angles of 109−110°, and ellipsometric thicknesses of 2.1 ± 0.1 and 2.2 ± 0.1 nm for monolayers derived from hexadec-3-en-1-yne and 1-hexadecyne, respectively, compare well with literature values (111° and 2.1 nm for 1-hexadecyne) and confirm the high quality of both organic monolayers.[35] The theoretical layer thickness can be determined via eq 1 (see the Supporting Information for derivation). By inserting a tilt angle (θ) of 30°, which is the experimentally determined tilt angle of high-quality organic monolayers on gold,[54] a theoretical thickness of 1.90 nm for hexadecenyl and 1.89 nm for hexadecadienyl monolayers was calculated. This is somewhat lower than the ellipsometric values, which is likely caused by the assumed tilt angle of 30°. A smaller tilt angle, indicating more upright positioned chains, will result in thicker layers.

1-hexadecyne (nm):

$$d_{\text{Th}} = 0.188 + 1.772\cos\theta + 0.156\sin(35.5 + \theta) \quad (1a)$$

hexadeca-3-en-1-yne (nm):

$$d_{\text{Th}} = 0.188 + 1.765\cos\theta + 0.156\sin(35.5 + \theta) \quad (1b)$$

ATR measurements show the antisymmetric and symmetric CH₂ stretching vibrations at 2918.8 and 2849.4 cm⁻¹ (hexadecenyl), and 2917.6 and 2847.5 cm⁻¹ (hexadecadienyl), respectively, for both monolayers (see Figure 4). The value for hexadecenyl monolayers is in line with literature values[35] and is indicative of a highly ordered monolayer. In this regard, it should be noted that these hexadecadienyl monolayers have two methylene groups less for favorable interchain van der Waals interactions as compared to hexadecenyl monolayers and even four methylene groups less as compared to hexadecyl monolayers. Therefore, it is remarkable that such a highly ordered organic monolayer can be obtained with only 12 CH₂ groups (cf., dodecyl termination), especially when comparing these low wavenumbers with those of a dodecyl monolayer on H−Si(111) (2922 cm⁻¹).[35]

In addition, ATR measurements proved sensitive enough to capture the C=C stretch vibrations around 1600 cm⁻¹. A clear single peak is visible in the hexadecenyl spectrum, whereas hexadecadienyl gives two peaks. Simulations (vibrations obtained from G3 calculations, see paragraph 3) show that the denyl moiety gives rise to two peaks, and that one is indeed

shifted to higher wavenumbers, which is in good agreement with the ATR results (see Figure 4b). This result indicates terminal attachment of the 2-en-1-yne with retention of the double bonds upon monolayer formation. The C−H stretch vibration, however, is only visible in the hexadecadienyl layer (3016 cm⁻¹), which may be explained by the higher concentration (two double bonds instead of one).

To study the linkage to the Si(111) substrate in more detail, XPS C₁ₛ narrow scans were recorded. In addition, density functional theory (DFT) calculations were used to calculate the binding energies of the distinct carbon atoms in the linkage. As shown in Figure 5A and B, both C₁ₛ spectra are deconvoluted into three contributions. The components at 283.8, 285.0, and 285.7 eV have been assigned to the carbons directly attached to the relatively electropositive silicon (C−Si, E_{calc} = 283.9 eV), the aliphatic carbons (C−C, E_{calc} = 285.0 eV), and the more electronegative sp² hybridized carbons (C=C, E_{calc} = 285.6 and 285.8 eV), respectively. In combination with DFT calculations on other possible binding conformations (see the Supporting Information), the relative intensities of these distinct carbons disclose the linkage of both monolayer types to the H−Si(111) surface, that is, 1:12:3 for hexadec-1-en-3-yne-derived monolayers with a Si−C=C−C=C linkage and 1:14:1 for 1-hexadecyne-derived monolayers with a Si−C=C linkage. In addition, in the Si₂ₚ narrow scans obtained for the dienyl and alkenyl layers (see Figure 5C and D), no silicon oxide was identified in the 101−103.5 eV region. This again confirms the monolayer quality and its ability to prevent appreciable oxidation of the underlying Si substrate.[36]

Moreover, to extract the packing densities, also the exact composition of monolayers was determined by quantitative XPS measurements. To overcome the signal dependency on the orientation of the crystal, that is, to remove any influence of X-ray diffraction, the XPS samples were rotated 360° around the surface normal, in steps of 10°.[35,39] The obtained C/Si ratios display the expected periodicity of 120° and reveal an increased amount of carbon for the hexadecadienyl monolayers as compared to the hexadecenyl monolayers (Table 1). The surface coverage and monolayer thickness were calculated from these C/Si ratios equations 2 and 3:[27,56]

Table 1. Quantitative XPS Data: Atomic C/Si Ratios, Resulting Monolayer Thickness, and Surface Coverage of Hexadecadienyl and Hexadecenyl Monolayers on H−Si(111)

reactant	XPS C_{1s}/Si_{2p} ratios	surface coverage %
C₁₆ enyne	40.2/59.8 (±1.0/1.0)[a]	63%
C₁₆ alkyne	37.7/62.3 (±1.2/1.2)[a]	59%

[a]C₁ₛ/Si₂ₚ ratios and errors based on three separately prepared fully characterized monolayers.

Thickness:

$$d_{\text{ML}}(\text{Å}) = \lambda_{\text{ML}}^{\text{Si}}\sin(\varphi)\ln(1 + C/Si) \quad (2)$$

Surface coverage:

$$\theta_{\text{ML}} = \frac{d_{\text{ML}} \times D_{\text{Au}}}{d_{\text{TH}(30)} \times D_{\text{Si}}} \quad (3)$$

in which $\lambda_{\text{ML}}^{\text{Si}}$ is the attenuation length of Si₂ₚ photoelectron in the organic monolayer (39.5 Å), and ϕ is the angle between the surface plane and the detector (90°). The surface coverage is

estimated by comparison to the literature value of a fully characterized alkanethiol monolayer on gold, where d_{TH} is the theoretical thickness of an organic monolayer on H−Si(111) with a tilt angle of 30° (1.90 and 1.89 nm for alkenyl and dienyl layers, respectively), and D_{Si} and D_{Au} are the number of sites per cm (7.8×10^{14} and 4.65×10^{14} cm^{-2}, respectively).[35,39] From the results in Table 1, it shows that the dienyl layers, with a surface coverage of 63% (±1%), are significantly more densely packed than the hexadecenyl monolayers, while the XPS-derived thickness of both layers is the same within the experimental error (1.9 ± 0.1 and 2.0 ± 0.1 nm, for enyne-derived and alkyne-derived C$_{16}$ monolayers, respectively). The thickness and surface coverage of 59% for the hexadecenyl monolayers are in excellent agreement with previous findings.[35] These results clearly show that, besides an increased reactivity, the 3-en-1-yne moiety also leads to a significant higher surface coverage, fulfilling both prerequisites for improvement of quality in monolayers.

Finally, to investigate the ordering of the monolayer in more detail, high-quality near-edge X-ray absorption fine structure (NEXAFS) measurements were performed. NEXAFS spectra provide information about the electronic structure of the surface species by measuring characteristic absorption resonances corresponding to electronic transitions from atomic core levels to unoccupied molecular orbitals.[55] Carbon K-edge spectra for the hexadecadienyl and hexadecenyl layers on silicon, acquired at 70°, 55°, and 20°, are presented in Figure 6
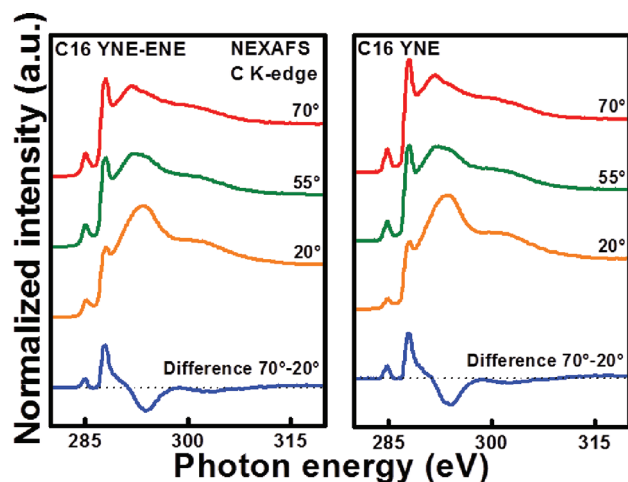
Figure 6. NEXAFS carbon K-edge spectra for hexadecadienyl and hexadecenyl monolayers on Si(111), acquired at 70°, 55°, and 20°. The difference spectra between the 70° and the 20° data are shown in blue.

along with the difference between the 70° and 20° spectra. Because radiation damage from the X-ray would also be visible

in this spectral range,[56] a careful beam damage study was performed to rule out this possibility.[57] The adsorption near 285.0 eV, π^*(C═C) clearly indicates a resonance of the aromatic alkene moieties, whereas the strong Rydberg/C−H (R*) resonance near 287.9 eV and the broad σ^* resonances are related to the alkyl chains and the C−C bonds at higher photon energies, respectively. The spectra show no signs of chemical impurities such as C═O, nor any traces of unreacted C≡C moieties (expected near 285.9 eV) for any of the monolayers.[55,58−61] The pronounced linear dichroism for the C═C, C−C, and C−H related resonances (highlighted by the 70° − 20° difference spectra) indicates significant order and molecular alignment in both monolayers. The positive polarity of the observed difference peaks for the π^* resonance implies a strongly tilted orientation of the π^*(C═C) orbitals, which is expected for an upright chain orientation, because the π^*(C═C) orbitals are perpendicular to the C═C−C plane. The R* features also show an appreciable positive linear dichroism, while the C−C difference peaks are negative, which is again a clear indication of an upright orientation of the alkyl chain.

A quantitative analysis of the C K-edge NEXAFS spectra was performed to determine the average molecular tilt and twist angles. The orientation of the carbon chains with respect to the surface normal was determined using the R* transitions. The intensities of these resonances as a function of the X-ray incidence angle Θ were evaluated using literature procedures for a planar orbital.[55] This analysis yields average tilt angles versus the surface normal of 28° ± 5° and 25° ± 5° for dienyl and alkenyl layers, respectively. These values are similar to those observed for alkane thiols on gold (28°).[62] In addition, these NEXAFS data can be used (via eq 2) to derive monolayer thicknesses, and these agree within experimental error with the XPS thicknesses.

The tilt angle of the alkene π^*(C═C) orbitals was determined using the π^* resonance intensity variations and a standard methods for vector orbitals.[55] The orientations of the orbitals (ρ) were found to be 66° ± 5° and 76° ± 5° for dienyl and alkenyl chains, respectively. These values can be used, together with eq 4, to determine the twist angle of the chains.[63] The twist angle ψ can be described as the rotation over the long molecular axis of the chains.

$$\rho = \arccos(\sin\phi\cos\psi) \qquad (4)$$

This evaluation yields twist angles of $\psi = 60°$ and $\psi = 45°$ for dienyl and alkene chains, respectively. These values are in line with geometries observed for related alkanethiols on gold (53°) and other metal surfaces.[54] Overall, the NEXAFS data indicate that the structure of the hexadecadienyl and hexadecenyl layers is very similar. Both are densely packed, highly ordered, and contamination free. The structure and orientation of the monolayers are also very similar to the binding geometry observed for alkanethiols on gold.

Table 2. Calculated Characteristics of Hexadecenyl and Hexadecadienyl Monolayers on H−Si(111)

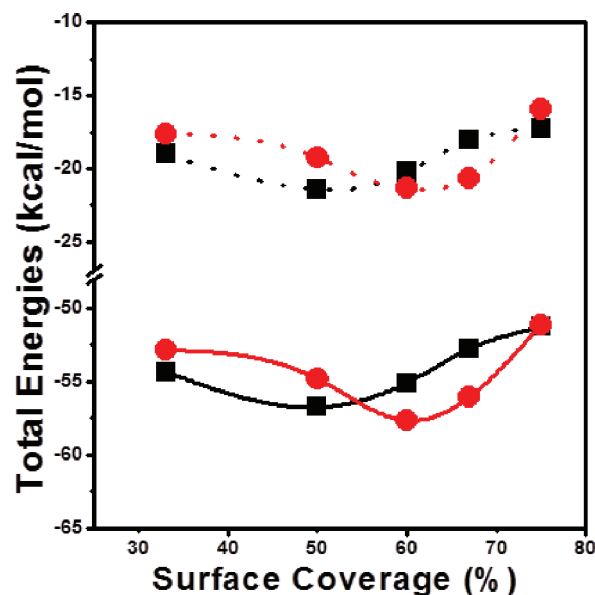|	hexadecenyl			hexadecadienyl		
unit cell	thickness (nm)	tilt angle chain	∠Si−C═C (in deg)	thickness (nm)	tilt angle chain	∠Si−C═C (in deg)
33A	1.2	61 ± 2	123 ± 1	1.3	56 ± 2	121 ± 1
50A	1.7	48 ± 2	123 ± 2	1.8	26 ± 4	124 ± 2
60A	2.0	19 ± 6	125 ± 3	1.8	27 ± 3	124 ± 4
67A	2.0	17 ± 2	124 ± 3	2.0	11 ± 4	126 ± 3
75A	2.1	8 ± 3	124 ± 3	2.0	5 ± 3	127 ± 2

3. Molecular Modeling. The obtained difference in surface coverage stimulated us to perform a comparative molecular modeling study of monolayers derived from 1-hexadecyne and hexadec-3-en-1-yne. Unit cells containing hexadecadienyl and hexadecenyl (both C_{16}) chains were constructed and used to create large simulation cells with various substitution percentages and substitution patterns analogous to those described in literature.[38,40,41,64−66] Energy minimizations were performed using a polymer consistent force field (PCFF) with high-convergence criteria and periodic boundaries conditions to eliminate the edge effects and to mimic an infinitely large monolayer.

The structure of the resulting optimized monolayers was compared in detail with the available experimental data. Reported data are the average observed for the chains (48 at 33% coverage to 108 at 75% coverage) in the periodically repeating unit cells at a specific substitution pattern. As shown in Table 2 for one of the substitution patterns (arbitrarily labeled A; see for other patterns and corresponding data the Supporting Information), at a coverage of approximately 60−67%, the alkenyl and dienyl layers display a calculated thickness of 1.9 and 2.0 nm, respectively. These values agree with the thicknesses derived from the XPS and NEXAFS measurements discussed above (1.9 ± 0.1 nm for both layers). The differences between both types of layers become clear after comparison of the tilt and the layer thicknesses at the various surface coverages. At low coverage (33−50%), the dienyl chains are more upright oriented than the alkenyl chains, resulting in a higher layer thickness. However, the tilt angles for alkenyl layers decrease rapidly when going to a higher surface coverage, while the dienyl layers show a more gradual decrease. This behavior can be explained by the rigidity of the dienyl moiety, which is caused by the two double C=C bonds and their overlapping p-orbitals, which keep the four carbons in an almost planar conformation (typical dihedral C=C−C=C ≈ 170° for 33−60% coverage). At low coverage, the dienyl will thus keep its upright orientation, whereas the alkenyl moiety has more rotational freedom, resulting in a more flat orientation of alkyne-derived monolayers. Both layers show a slight increase of the Si−C=C bond angles with increasing coverage, likely caused by the optimization of the interchain van der Waals interactions between CH_2 moieties at the expense of such minor distortions at the surface.

Next to the structural parameters of the monolayers, also the packing energies were determined. After optimization of the layer, the chains were cut loose from the surface. The carbon atoms that were attached to silicon were left uncapped because capping with hydrogen led to distortion of the geometry. The resulting dangling carbon bonds were subsequently neglected by the used PCFF force-field. The average packing energy per chain was then calculated according to:

$$E_{\text{packing}} = \frac{E_{\text{chains}}}{n} - E_{\text{single}} \qquad (5)$$

in which E_{chains} is the total packing energy of the layer, n is the number of chains in the layer, and E_{single} is the energy of a separately optimized chain.[64] The resulting average packing energies per chain are shown in Figure 7 (dotted lines). At low surface coverage, hexadecenyl layers are energetically more favorable than dienyl layers. This difference can be explained by the upright position of the rigid dienyl moiety that pushes the CH_2 chain up, to an orientation in which the $\pi-\pi$ overlap of the resulting diene moiety competes with the interchain van der

Figure 7. Packing energy (····) and total energy (—) per chain for hexadecenyl (■) and hexadecadienyl (●) monolayers, as a function of surface coverage.

Waals interactions between CH_2 moieties. For the alkyne-derived monolayer, such competition is absent, yielding a more flat orientation of the CH_2 chains with concomitantly increased attractive van der Waals interactions.

The optimum for the C_{16} alkenyl layers is found around 50% coverage, while for the C_{16} dienyl monolayer this is close to 60%. This difference seems to correspond to the experimental finding that hexadecadienyl layers can achieve a higher surface coverage (63%) than hexadecenyl layers (59%). However, given the experimental and modeling uncertainties, the significance is not that pronounced. This can largely be attributed to the volumes of the atoms close to the silicon surface (−CH=CH−CH=CH− versus −CH=CH−CH_2−CH_2−), which for the −CH=CH−CH=CH− moiety is ∼5% smaller, with concomitant reduction of steric repulsions as increased surface coverages.

The optimum packing, however, is still lower than the experimentally observed packing of both the alkenyl and the dienyl layers. The likely dominant part of the explanation for this phenomenon lies in the fact that the binding of the chains to the surface is energetically highly favorable and irreversible, yielding an experimental density that is higher than the optimum for the noncovalent interchain interactions.

The second aspect controlling the experimentally observed packing density relates to the Si−C binding energy. For the monolayers under study, this was calculated via high-quality G3 ab initio calculations of the reaction of 1-pentyne and pent-3-en-1-yne with a small hydrogen-terminated silicon cluster ($HSi(SiH_3)_3$), analogous to literature procedures.[64,65] For fully relaxed structures, this would favor the reaction of the enyne by 2.6 kcal mol^{-1}. However, the situation is slightly more complicated, as for varying coverages the precise structures near the surface vary slightly. To take this into account properly, the product geometries for the G3 calculations were isolated from the PCFF-optimized monolayer structures discussed earlier. Isolated Si_4 clusters were cut out of the surface slabs, and the chains were truncated to five carbon atoms, to lower the computational cost. The atoms were then

constrained, to perform single-point G3 energy calculations (see the Supporting Information for a more detailed description). The binding energy was then calculated as the difference of the energy of the chain attached to the surface and the fully relaxed reactant complexes, and corrected for the energy contribution of the deformation of the C_5 chain, according to literature procedures.[64] Figure 7 (continuous lines) then shows the sum of packing and binding energies at the various degrees of surface coverage for enyne-derived and alkyne-derived C_{16} monolayers. This profile of the total energy resembles the profile of the packing energy, but shows a more distinct preference for the reactivity of the C_{16} enyne. For the calculated total energies of 60% and 67%, that is, close to what is experimentally observed, the energy gap between the alkenyl and the dienyl layers increases to 2.5 and 3.2 kcal mol^{-1}. This overall higher reaction exothermicity and higher optimum packing density for enyne-derived monolayers fits very well with the experimental observation of the faster reaction of the C_{16} enyne than of hexadecyne (Figure 1), and the observed higher denser packing of the dienyl layers (Figure 4).

CONCLUSIONS

We successfully developed a novel precursor, hexadeca-3-en-1-yne ($HC{\equiv}C-HC{=}CH-C_{12}H_{25}$), for the formation of high-quality monolayers on H-terminated silicon surfaces. Detailed kinetics studies show that this enyne reacts faster than the corresponding C_{16} alkyne, while quantitative XPS studies show that the resulting dienyl monolayers also display a higher packing density than had been reported up to now on H−Si(111). Infrared and NEXAFS measurements confirm the formation of highly ordered, densely packed enyne-derived monolayers. Finally, a molecular modeling study (combination of molecular mechanics calculations on complete monolayers and G3 ab initio calculations on well-defined model systems) shows that for C_{16} monolayers an enyne-derived monolayer is both more stable and more densely packed than the monolayer derived from the corresponding C_{16} alkyne (hexadecyne).

This enhanced monolayer quality and rate of formation of enyne-derived monolayers, as compared to the best performing reagent up to now (1-alkynes), makes enynes $HC{\equiv}C-HC{=}CH-R$ the agent of choice if a supreme monolayer quality is desired, which also enhances the stability of the oxide-free silicon interface. This development further increases the chance of a successful application of organic monolayers on silicon in electronic and biosensor devices.

ASSOCIATED CONTENT

Ⓢ Supporting Information
Theoretical derivation of monolayer thickness, detailed procedure of monolayer simulations, DFT calculations of binding energy, full IRRAS spectrum, and full ref 34. This material is available free of charge via the Internet at http://pubs.acs.org.

AUTHOR INFORMATION

Corresponding Author
*Phone: +31-317-482361. Fax: +31-317-484914. E-mail: han.zuilhof@wur.nl.

Notes
The authors declare no competing financial interest.
[⊥]These authors contributed equally.

REFERENCES

(1) Gooding, J. J.; Ciampi, S.; Harper, J. B. *Chem. Soc. Rev.* **2010**, *39*, 2158−2183.
(2) Buriak, J. M. *Chem. Rev.* **2002**, *102*, 1271−1308.
(3) Yonezawa, T.; Shirahata, N.; Hozumi, A. *Chem. Rec.* **2005**, *5*, 145−159.
(4) Gooding, J. J.; Ciampi, S. *Chem. Soc. Rev.* **2011**, *40*, 2704−2718.
(5) Rijksen, B.; Caipa Campos, M. A.; Paulusse, J. M. J.; Zuilhof, H. In *Encyclopedia of Radicals in Chemistry, Biology and Materials*; Chatgilialoglu, C., Struder, A., Eds.; Wiley: Chichester, 2012.
(6) Scheres, L.; ter Maat, J.; Giesbers, M.; Zuilhof, H. *Small* **2010**, *6*, 642−650.
(7) Linford, M. R.; Fenter, P.; Eisenberger, P. M.; Chidsey, C. E. D. *J. Am. Chem. Soc.* **1995**, *117*, 3145−55.
(8) Sieval, A. B.; Huisman, C. L.; Schoenecker, A.; Schuurmans, F. M.; Van der Heide, A. S. H.; Goossens, A.; Sinke, W. C.; Zuilhof, H.; Sudhölter, E. J. R. *J. Phys. Chem. B* **2003**, *107*, 6846−6852.
(9) Cicero, R. L.; Linford, M. R.; Chidsey, C. E. D. *Langmuir* **2000**, *16*, 5688−5695.
(10) Shestopalov, A. A.; Clark, R. L.; Toone, E. J. *Langmuir* **2010**, *26*, 1449−1451.
(11) Terry, J.; Mo, R.; Wigren, C.; Cao, R. Y.; Mount, G.; Pianetta, P.; Linford, M. R.; Chidsey, C. E. D. *Nucl. Instrum. Methods Phys. Res., Sect. B* **1997**, *133*, 94−101.
(12) Wang, X. Y.; Ruther, R. E.; Streifer, J. A.; Hamers, R. J. *J. Am. Chem. Soc.* **2010**, *132*, 4048−4049.
(13) Robins, G.; Stewart, P.; Buriak, M. *Chem. Commun.* **1999**, 2479−2480.
(14) Belanger, D.; Pinson, J. *Chem. Soc. Rev.* **2011**, *40*, 3995−4048.
(15) Niederhauser, T. L.; Jiang, G. L.; Lua, Y. Y.; Dorff, M. J.; Woolley, A. T.; Asplund, M. C.; Berges, D. A.; Linford, M. R. *Langmuir* **2001**, *17*, 5889−5900.
(16) Yang, L.; Lua, Y.-Y.; Tan, M.; Scherman, O. A.; Grubbs, R. H.; Harb, J. N.; Davis, R. C.; Linford, M. R. *Chem. Mater.* **2007**, *19*, 1671−1678.
(17) Buriak, J. M.; Stewart, M. P.; Geders, T. W.; Allen, M. J.; Choi, H. C.; Smith, J.; Raftery, D.; Canham, L. T. *J. Am. Chem. Soc.* **1999**, *121*, 11491−11502.
(18) Jin, H.; Kinser, C. R.; Bertin, P. A.; Kramer, D. E.; Libera, J. A.; Hersam, M. C.; Nguyen, S. T.; Bedzyk, M. J. *Langmuir* **2004**, *20*, 6252−6258.
(19) Scheres, L.; Arafat, A.; Zuilhof, H. *Langmuir* **2007**, *23*, 8343−8346.
(20) Caipa Campos, M. A.; Paulusse, J. M. J.; Zuilhof, H. *Chem. Commun.* **2010**, *46*, 5512−5514.
(21) Popoff, R. T. W.; Asanuma, H.; Yu, H. Z. *J. Phys. Chem. C* **2010**, *114*, 10866−10872.
(22) Seitz, O.; Bocking, T.; Salomon, A.; Gooding, J. J.; Cahen, D. *Langmuir* **2006**, *22*, 6915−6922.
(23) Seitz, O.; Vilan, A.; Cohen, H.; Hwang, J.; Haeming, M.; Schoell, A.; Umbach, E.; Kahn, A.; Cahen, D. *Adv. Funct. Mater.* **2008**, *18*, 2102−2113.
(24) Yaffe, O.; Scheres, L.; Puniredd, S. R.; Stein, N.; Biller, A.; Lavan, R. H.; Shpaisman, H.; Zuilhof, H.; Haick, H.; Cahen, D.; Vilan, A. *Nano Lett.* **2009**, *9*, 2390−2394.

(25) Zigah, D.; Herrier, C.; Scheres, L.; Giesbers, M.; Fabre, B.; Hapiot, P.; Zuilhof, H. *Angew. Chem., Int. Ed.* **2010**, *49*, 3157−3160.

(26) Chatgilialoglu, C. *Organosilanes in Radical Chemistry*; John Wiley & Sons ltd: Chichester, England, 2004.

(27) Chatgilialoglu, C.; Guarini, A.; Guerrini, A.; Seconi, G. *J. Org. Chem.* **1992**, *57*, 2207−2208.

(28) Wayner, D. D. M.; Wolkow, R. A. *J. Chem. Soc., Perkin Trans. 2* **2002**, 23−34.

(29) Lehner, A.; Steinhoff, G.; Brandt, M. S.; Eickhoff, M.; Stutzmann, M. *J. Appl. Phys.* **2003**, *94*, 2289−2294.

(30) Sun, Q.-Y.; de Smet, L. C. P. M.; van Lagen, B.; Wright, A.; Zuilhof, H.; Sudhölter, E. J. R. *Angew. Chem., Int. Ed.* **2004**, *43*, 1352−1355.

(31) Rijksen, B.; Zuilhof, H., submitted.

(32) Takeuchi, N.; Kanai, Y.; Selloni, A. *J. Am. Chem. Soc.* **2004**, *126*, 15890−15896.

(33) Lalevée, J.; Blanchard, N.; Graff, B.; Allonas, X.; Fouassier, J. P. *J. Organomet. Chem.* **2008**, *693*, 3643−3649.

(34) Frisch, M. J.; et al. *Gaussian 09*, revision A.1; Gaussian, Inc.: Wallingford, CT, 2009.

(35) Scheres, L.; Giesbers, M.; Zuilhof, H. *Langmuir* **2010**, *26*, 4790−4795.

(36) Puniredd, S. R.; Assad, O.; Haick, H. *J. Am. Chem. Soc.* **2008**, *130*, 9184−9185.

(37) Nemanick, E. J.; Solares, S. D.; Goddard, W. A.; Lewis, N. S. *J. Phys. Chem. B* **2006**, *110*, 14842−14848.

(38) Sieval, A. B.; van den Hout, B.; Zuilhof, H.; Sudhölter, E. J. R. *Langmuir* **2001**, *17*, 2172−2181.

(39) Wallart, X.; De Villeneuve, C. H.; Allongue, P. *J. Am. Chem. Soc.* **2005**, *127*, 7871−7878.

(40) Pei, Y.; Ma, J.; Jiang, Y. *Langmuir* **2003**, *19*, 7652−7661.

(41) Zhang, L.; Wesley, K.; Jiang, S. *Langmuir* **2001**, *17*, 6275−6281.

(42) Barone, V.; Cacelli, I.; Ferretti, A.; Monti, S.; Prampolini, G. *J. Phys. Chem. C* **2011**, *115*, 4145−4154.

(43) Sano, H.; Maeda, H.; Ichii, T.; Murase, K.; Noda, K.; Matsushige, K.; Sugimura, H. *Langmuir* **2009**, *25*, 5516−5525.

(44) Hacker, C. A.; Anderson, K. A.; Richter, L. J.; Richter, C. A. *Langmuir* **2004**, *21*, 882−889.

(45) Miller, J. A.; Zweifel, G. *J. Am. Chem. Soc.* **1983**, *105*, 1383−1384.

(46) Kim, T.; Crooks, R. M. *Tetrahedron Lett.* **1994**, *35*, 9501−9504.

(47) Xu, Z.; Byun, H. S.; Bittman, R. *J. Org. Chem.* **1991**, *56*, 7183−7186.

(48) Sieval, A. B.; Linke, R.; Zuilhof, H.; Sudhölter, E. J. R. *Adv. Mater.* **2000**, *12*, 1457−1460.

(49) Allongue, P.; de Villeneuve, C. H.; Morin, S.; Boukherroub, R.; Wayner, D. D. M. *Electrochim. Acta* **2000**, *45*, 4591−4598.

(50) Yang, M.; Teeuwen, R. L. M.; Giesbers, M.; Baggerman, J.; Arafat, A.; De Wolf, F. A.; Van Hest, J. C. M.; Zuilhof, H. *Langmuir* **2008**, *24*, 7931−7938.

(51) de Smet, L. C. P. M.; Pukin, A. V.; Sun, Q.-Y.; Eves, B. J.; Lopinski, G. P.; Visser, G. M.; Zuilhof, H.; Sudhölter, E. J. R. *Appl. Surf. Sci.* **2005**, *252*, 24−30.

(52) Brunner, H.; Mayer, U.; Hoffmann, H. *Appl. Spectrosc.* **1997**, *51*, 209−217.

(53) Hasegawa, T.; Takeda, S.; Kawaguchi, A.; Umemura, J. *Langmuir* **1995**, *11*, 1236−1243.

(54) Love, J. C.; Estroff, L. A.; Kriebel, J. K.; Nuzzo, R. G.; Whitesides, G. M. *Chem. Rev.* **2005**, *105*, 1103−1169.

(55) Stöhr, J. *NEXAFS Spectroscopy*; Springer-Verlag: Berlin, 1992; Vol. 25.

(56) Weidner, T.; Shaporenko, A.; Ballav, N.; Ulman, A.; Zharnikov, M. *J. Phys. Chem. C* **2008**, *112*, 1191−1198.

(57) For the beam damage study at the C K-edge, the 280−320 eV energy range was repeatedly scanned and analyzed. In addition, the partial electron yield at 285 eV was monitored over time to rule out damage-related changes in the first seconds. No changes in the spectra were observed within 15 min, which is more than the exposure time in the longest carbon scans performed within this work. This studied proved that the pre-edge feature observed near 285 eV is not caused by beam damage.

(58) Outka, D. A.; Stöhr, J.; Rabe, J. P.; Swalen, J. D. *J. Chem. Phys.* **1988**, *88*, 4076.

(59) Weiss, K.; Bagus, P. S.; Wöll, C. *J. Chem. Phys.* **1999**, *111*, 6834−6845.

(60) Väterlein, P.; Fink, R. *J. Chem. Phys.* **1998**, *108*, 3313.

(61) Cabarcos, O. M.; Shaporenko, A.; Weidner, T.; Uppili, S.; Dake, L. S.; Zharnikov, M.; Allara, D. L. *J. Phys. Chem. C* **2008**, *112*, 10842−10854.

(62) Laibinis, P. E.; Whitesides, G. M. *J. Am. Chem. Soc.* **1992**, *114*, 1990−1995.

(63) Rong, H.-T. F., S.; Yang, Y.-J.; Zharnikov, M.; Buck, M.; Wuhn, M.; Wöll, C.; Helmchen, G. *Langmuir* **2001**, *17*, 1582−1593.

(64) Scheres, L.; Rijksen, B.; Giesbers, M.; Zuilhof, H. *Langmuir* **2011**, *27*, 972−980.

(65) Sieval, A. B.; van den Hout, B.; Zuilhof, H.; Sudhölter, E. J. R. *Langmuir* **2000**, *16*, 2987−2990.

(66) Yuan, S.-L.; Cai, Z.-T.; Jiang, Y.-S. *New J. Chem.* **2003**, *27*, 626−633.